INT. J. REMOTE SENSING, 1997, VOL. 18, NO. 11, 2383–2401

Investigation of the maximum Normalized Difference Vegetation Index (NDVI) and the maximum surface temperature (T_s) AVHRR compositing procedures for the extraction of NDVI and T_s over forest

D. P. ROY†

Joint Research Centre (JRC), Space Applications Institute, EMAP, I-21020 Ispra (Va), Italy

(*Received 21 August 1995; in final form 25 November 1996*)

Abstract. An investigation into the impact of the maximum Normalized Difference Vegetation Index (NDVI) and the maximum surface temperature (T_s) compositing procedures (MaN and MaT respectively) upon retrieved NDVI and T_s values extracted from forested areas located across eight months of cloud-screened European AVHRR data is described. NDVI values are found to be significantly higher and generally less variable when they are extracted from MaN rather than from MaT composites and T_s values are found to be significantly higher and generally less variable when they are extracted from MaT rather than from MaN composites. The impact of these differences is illustrated within the context of a European forest/non-forest classification that uses both NDVI and T_s data. Higher potential forest/non-forest classification accuracies are found using NDVI data extracted from the MaN composites and T_s data extracted from the MaT composites than from any other combination of composited data. The findings indicate that inappropriate selection of a compositing procedure may have a significant impact upon the subsequent application of NDVI and/or T_s data.

1. Introduction

Satellite measurements made at visible and thermal wavelengths may be used to characterize land cover and derive biophysical parameters in support of many areas of research including global change (Running *et al.* 1994). At present only the AVHRR sensor provides data of an appropriate spatial and temporal resolution to support studies at regional to global scales (Moody and Strahler 1994). The utility of AVHRR data is reduced by a variety of non-constant factors that include variable sensor response over the wide AVHRR field-of-view, and cloud and atmospheric contamination. The variable AVHRR sensor response is caused by angular sensing and illumination variations across the image swath (Holben 1986) combined with the anisotropy of reflectance from most natural surfaces (Pinty and Verstraete 1992) and the atmosphere (Kaufman 1989). Correction for these effects requires a comprehensive knowledge of the surface and atmosphere bidirectional reflectance properties which are not usually available. Variable AVHRR sensor response may also be caused by the coarsening of spatial resolution at view angles further from nadir (Breaker 1990). Masking techniques are used to remove cloud contamination but are only partially useful as they cannot reliably detect cloud at a sub-pixel level

† Now at The Department of Geography, University of Maryland and NASA Goddard Space Flight Center, Code 922, Greenbelt, MD 20771, U.S.A.

(e.g., Davis *et al.* 1993, Cihlar 1994) and because they produce single data images with missing values (Moody and Strahler 1994). Atmospheric correction schemes are used to reduce atmospheric contamination (e.g., Tanré *et al.* 1990, Vermote *et al.* forthcoming) but over large areas their effectiveness is limited by the availability of data quantifying the atmospheric absorbing and scattering constituents. A practical and commonly used approach to improve the utility of AVHRR data is to apply a compositing procedure to a time series of co-registered data. Compositing procedures use compositing criteria that are designed to select from the time series only near-nadir pixel measurements that have reduced cloud and atmospheric contamination. This paper examines compositing procedures that use the maximum value of the Normalized Difference Vegetation Index and the maximum value of the apparent surface temperature as compositing criteria.

For land based studies the most commonly used compositing procedure uses the maximum value of the Normalized Difference Vegetation Index (NDVI). The NDVI is a well known spectral vegetation index defined as the difference between near-infrared and red reflectances divided by their sum (Curran 1983). The NDVI is related in a directly proportional manner to photosynthetic activity (Sellers 1985) and, when integrated over time, has been shown to correlate with above ground green biomass (Tucker *et al.* 1981, 1985, Goward and Dye 1987, Running and Nemani 1988). The NDVI is sensitive to atmospheric perturbations, cloud contamination, soil background and illumination and viewing geometry (Goward *et al.* 1991, Los *et al.* 1994, Epiphanio and Huete 1995, Liu and Huete 1995, Meyer *et al.* 1995). The maximum NDVI (MaN) compositing procedure was developed in an attempt to reduce some of these effects and is based on the assumption that signal contamination will depress NDVI values. Holben (1986) demonstrated that MaN compositing reduces cloud influences for a large range of viewing and illumination angles and for all aerosol conditions. He also showed that maximum NDVI values occur at near nadir viewing angles and small solar zenith angles where angular variations in the sensor response tend to be minimized. However, reflectance anisotropy can result in the selection of a pixel with a high NDVI caused by directional rather than atmospheric effects (Gutman 1987, Meyer *et al.* 1995) which may cause substantial radiometric variations in composited original channel data (D'Iorio *et al.* 1991). This effect may be exacerbated if the data are atmospherically corrected prior to compositing. Cihlar *et al.* (1994 b) observed a reduced NDVI variation with respect to view angle in atmospherically corrected data and therefore an increased probability of selecting off-nadir pixels using the MaN procedure. AVHRR data composited using the maximum NDVI have been used to classify regional to global scale vegetation cover types (Tucker *et al.* 1994, Justice *et al.* 1985, Prince and Tucker 1986, Townshend *et al.* 1987, Loveland *et al.* 1991, DeFries and Townshend 1994).

Recently, the utility of other compositing procedures for land based applications have been investigated (Cihlar *et al.* 1994 a). Maximum surface temperature (T_s) has been suggested (Cihlar *et al.* 1994 a) because clouds and shadows tend to decrease the apparent T_s in daytime satellite thermal infrared data (e.g., Cihlar 1987) and because apparent T_s decreases away from nadir with increasing atmospheric path length and thereby increased atmospheric attenuation (Wan and Dozier 1989). However, T_s varies rapidly in space and time as a complex function of surface properties (vegetation cover and structure, moisture status, emissivity), subsurface properties (conductivity, specific heat density) and atmospheric conditions (solar

radiation, wind speed) (Goward *et al.* 1985, Goward and Hope 1989, Norman *et al.* 1995). T_s is related, through the surface energy balance equation, to surface moisture availability and evapotranspiration as function of latent heat flux (e.g., Carlson *et al.* 1981, Taconet *et al.* 1986). Over bare soils T_s is highly correlated with surface moisture content but over vegetated surfaces the relation is more complex (Carlson *et al.* 1990). T_s is observed to be inversely proportional to the vegetation canopy cover because of a variety of factors (Lambin and Ehrlich 1996) that include latent heat transfer through evapotranspiration, and because of the lower heat capacity and thermal inertia of vegetation compared to that of soil (Gates 1980, Choudhury 1989, Goward and Hope 1989). This implies that the maximum T_s compositing procedure may preferentially select less densely vegetated pixels. However, over sparsely vegetated surfaces, the fraction of bare soil viewed by the sensor will decrease away from nadir, resulting in many cases in lower T_s and so a reduction in the likelihood of an off-nadir pixel being selected. Orbit variations in the time of satellite overpass and changes in the local solar time across the image swath may contribute to difficulties in interpreting satellite T_s measurements (Vogt 1995). The effective emissivity viewed by the sensor depends upon the view angle as well as on the anisotropy of the surface (Labed and Stoll 1991) and may result in the selection of a pixel with a high apparent T_s caused by directional rather than by surface effects. Despite these complicating factors, Cihlar *et al.* (1994 a) observed visually that the maximum T_s (MaT) procedure produced NDVI composites that more closely resembled a near-nadir cloud-free image than the MaN procedure.

This paper describes an empirical investigation into the impact of maximum NDVI (MaN) and maximum T_s (MaT) AVHRR compositing procedures upon retrieved NDVI and T_s values. It is expected that NDVI and T_s extracted from composited data will be sensitive to the type of compositing procedure that is applied. This is because the physical processes controlling NDVI and T_s are different and because NDVI and T_s are measured in different parts of the electromagnetic spectrum (reflected and emitted wavelengths respectively) where atmospheric scattering and absorption processes are very different (Price 1984, Kaufman 1989). Consequently a near-nadir atmospherically clear pixel selected using the MaN procedure may not be selected using the MaT procedure and vice-versa. Differences between the values of NDVI and between the values of T_s extracted from AVHRR data composited using the MaN and the MaT procedures may have an impact upon those applications that utilise composited NDVI and/or T_s data. The objective of this paper is to establish which of these compositing procedures are most suitable for the extraction of NDVI and T_s data over land. This is achieved by examination of the statistical characteristics of NDVI and T_s values extracted from MaN and MaT composites rather than by examination of the view angles and the cloud content of the composited data.

It is difficult to map land cover in detail at the scale of AVHRR imagery and so this investigation is performed with respect only to forest cover types. The investigation is performed using European coverage AVHRR data acquired over eight months to ensure a high variability of the biophysical variables (e.g., climatic, vegetation/ecosystem, soil/hydrology and topography) that can be expected to influence NDVI and T_s. The AVHRR data are processed independently into eight monthly MaN and eight monthly MaT composites. Values of NDVI and T_s are extracted from forest and non/forest pixels located in contiguous strata that characterize several different ecological/climatic regions and forest types found in the

composited data. Forest NDVI values extracted at the same locations from the MaN and from the MaT composites are compared statistically to characterize any differences that may be introduced by the two compositing procedures. Similarly forest T_s values extracted from the MaN and the MaT composites are compared. The comparisons are performed independently for each month of composited data and for all eight months of data. To reduce the effects of consistently cloudy data only cloud-free pixels are examined. In this way any differences observed between the MaN and MaT compositing procedures may be inferred as being due to differences between the physical processes controlling NDVI and T_s and to differences in the remotely-sensed measurement of these variables. The impact of the observed differences are illustrated within the context of a European forest/non-forest classification that utilizes NDVI and T_s data.

2. Remotely-sensed data

Daily European coverage AVHRR mosaics were selected from the data archive of the JRC MARS (Monitoring Agriculture with Remote Sensing) project (Meyer-Roux and Vossen 1993). In total 68 relatively cloud-free mosaics sensed from March to October of 1993 were selected. Each mosaic has an approximate surface area of 7·8 by 10^6 km^2 and covers the geographical area from the Portuguese coast to central Crete (west–east) and from Northern Algeria to Southern Norway (south–north).

An overview of the processing chain used to produce the AVHRR mosaics can be found in Vowles (1991). Each mosaic is composed of five channels of 2779 by 2343 pixels made from between approximately three to six afternoon pass NOAA-11 AVHRR LAC (1·1 km pixel) images. The 128 pixels lying at the ends of each AVHRR scanline (describing off-nadir view angles 48°–55°) are not used because of bidirectional reflectance effects and the extreme coarsening of spatial resolution found at these viewing angles. Standard radiometric calibrations are performed that account for sensor degradation using published coefficients (Rao and Chen 1994). Atmospheric corrections are performed using a modified version of the 5S code (Tanré *et al.* 1990) with standard atmospheric water vapour, oxygen and ozone data. AVHRR channel 1 (red: 0·58–0·68 μm) and channel 2 (near-infrared: 0·725–1·10 μm) are converted into apparent surface reflectances and AVHRR channels 4 and 5 (thermal infrared: 10·3–11·3 μm and 11·5–12·5 μm) are converted into brightness temperatures. AVHRR channel 3 (3·55–3·93 μm) is not used in this study. Surface cover information (land, sea, snow, cloud) are defined on a pixel by pixel basis by adaptive thresholding of the image data. The cloud detection procedure utilizes four separate methods based on the comparison of pixel values in different channels and the local gradient of the pixel values (Saunders and Kriebel 1988). The AVHRR images making up each mosaic are geometrically corrected using an orbit model and ground control located using a library of coastline templates (Muirhead and Malkawi 1989). The images are resampled into Albers map projection by nearest neighbour resampling with an output pixel dimension of 1·1 km^2. The geometric accuracy varies in each mosaic and is found empirically to be less than one to no more than approximately three pixels depending upon the proximity of a cloud-free coastline. These inaccuracies will introduce mosaic coregistration errors which may cause significant compositing errors. The compositing errors will be particularly apparent where the scene heterogeneity is high (Townshend *et al.* 1992) and in regions away from cloud-free coastlines where the mosaic geometric correction

accuracy is known to be poor. To reduce the impact of these problems only forest pixels selected from within large homogeneous forest areas are examined.

The time lag between the sensing of the images making up each mosaic may introduce reflectance and brightness temperature variability caused by changes in the position of the Sun and the time of day. The solar time differences in the selected mosaics are found to be less than two hours and are assumed to have a negligible impact upon T_s variability associated with warming or cooling over this period. Changes in the solar zenith upon the amount of incident solar radiation per unit surface area are assumed to cancel in the calculation of the NDVI (Holben and Justice 1981). However, the relative proportions of remotely-sensed canopy, understory, soil and shadow may change as function of the solar illumination and the viewing geometry (Pech and Davis 1987) and may introduce complex reflectance and emittance variations across each mosaic. These variations may not be removed completely by compositing, especially when only a small number of mosaics are used. Further, because the data are atmospherically corrected, the variation of NDVI and T_s with respect to view angle will be suppressed and therefore the probability of selecting an off-nadir pixel with a high NDVI or T_s value will be increased.

3. Compositing

The 68 AVHRR mosaics are processed *independently* into eight monthly MaN and eight monthly MaT composites (table 1). Only pixels flagged as being cloud-free are composited because pixels that are consistently cloudy within each monthly period will not be removed. The NDVI was calculated as the difference between the channel 2 and channel 1 reflectances divided by their sum (Curran 1983). Apparent T_s was calculated using a split-window technique modified for land surfaces with brightness temperatures derived from channels 4 and 5 and assuming a surface emissivity in both channels of 0·96 (Price 1984). The split-window technique is designed to reduce atmospheric water vapour attenuation in the thermal infrared and corrects for localized atmospheric variations. The monthly MaN composites are composed of a channel of maximum NDVI values and the original AVHRR image channels selected on a pixel by pixel basis from the mosaics with the maximum NDVI. Similarly, the monthly MaT composites are composed of a channel of maximum T_s values and the original AVHRR image channels selected from the mosaics with the maximum T_s.

Table 1. Daily European coverage AVHRR mosaics selected for compositing into eight monthly composites.

Month	Selected days of month of 1993												Total
March	3	8	13	15	20	21	26	30					8
April	1	7	10	15	16	22	25	27	28	29	30		11
May	5	10	11	12	17	23							6
June	10	12	20	26	27	28	30						7
July	1	4	5	7	12	16	23	24	29	31			10
August	1	2	7	8	14	15	16	17	23	25	26	31	12
September	1	4	9	16	19	23	25						7
October	4	5	18	19	21	27	29						7
											Grand Total		68

4. Forest and non-forest pixel location

Forest and non-forest pixels are located in the composite data using Geographical Information System map overlay techniques. The pixels are selected from 82 contiguous strata that characterize different ecological/climatic regimes and forest cover types found in the composite data. The pixel locations are defined within each stratum by examination of a binary forest/non-forest map. The forest/non-forest map is masked with a map of urban/non-urban regions to ensure that only non-urban (i.e., vegetation and soil) pixels are selected.

The contiguous forest strata are extracted from a vector database defined by a recent study to regionalise Europe into major ecological/climatic regions and homogeneous forest strata (European Commission 1995). Six ecological/climatic regions, 12 transition regions and an additional conglomerate region of mountainous area were defined at a scale of 1 : 2·5 million using climatic, soil and topographic data. The regions were sub-divided into 115 homogeneous forest strata by consideration of six ranked forest variables, the two most important being forest species composition and stand density. The geographical area covered by the AVHRR composite data contains 82 homogeneous forest strata and 13 ecological/climatic regions, transition regions and conglomerate mountainous regions. The smallest forest stratum has an area of 3·3 by 10^3 km^2 and the largest has an area of 2·9 by 10^5 km^2. The vector data defining the forest strata are transformed into coregistration with the forest/non-forest map to enable selection of forest and non-forest pixels within each stratum.

The binary forest/non-forest map was produced by unsupervised classification of 72 uncomposited daily AVHRR-LAC images selected from 1989 to 1992 (Hausler *et al.* 1993). Changes in the forest cover at the scale of AVHRR imagery between this period and 1993 are assumed to be negligible. The overall binary forest/non-forest map classification accuracy is 82·5 per cent (Hausler *et al.* 1993). The map is filtered using a morphological filter (Serra 1986) to ensure that only large homogeneous forest areas are selected. In this way it is hoped that errors of commission in the forest/non-forest map and the impact of any compositing errors caused by poor mosaic coregistration will be reduced. The forest/non-forest map is filtered in two different ways to produce separate forest and non-forest maps. The forest map is produced by removing the two outermost forest boundary pixels and isolated forest areas less than five pixels wide. The non-forest map is produced by enlarging the boundaries of the forest areas by two pixels and then labelling the remaining non-forest pixels. These maps are masked with a co-registered 1 : 1·0 million scale map of urban regions extracted from the Digital Chart of the World database (ESRI 1993). To reduce cartographic errors that may be present in this database the urban regions are enlarged by buffering their boundaries by 2 km (approximately two AVHRR pixels).

Forest and non-forest pixels are sampled randomly in space without replacement from the filtered forest and non-forest maps respectively. The sampling is performed independently in each stratum from the non-urban regions. Where possible 500 forest and 500 non-forest pixels are sampled from each stratum. In some strata less than 500 forest pixels are available because of sparse forest cover. The coordinates of the selected pixels are transformed into the coordinate system of the AVHRR composited data and are rounded to the nearest pixel.

5. Extraction of forest and non-forest NDVI and T_s data from monthly MaN and MaT composites

Values of NDVI and T_s are extracted from each monthly MaN and MaT composite at the selected forest and non-forest pixel locations. The NDVI values are extracted

from the maximum NDVI channel of each MaN composite and are calculated from the original image channels (channels 1 and 2) of the MaT composites. The T_s values are extracted from the maximum T_s channel of each MaT composite and are calculated from the original image channels (channels 4 and 5) of the MaN composites. In some strata less than 500 forest and 500 non-forest NDVI and T_s values are available because of missing composite data associated with consistently cloudy mosaic data. The total number of pairs of NDVI and T_s values extracted from each monthly MaN and MaT composite are summarized in table 2.

6. Analyses

The statistical distributions of forest NDVI values extracted at the same locations from the MaN and from the MaT composites are compared to characterize any differences that may be introduced by the two compositing procedures. Similarly forest T_s values extracted at the same locations from the MaN and the MaT composites are compared. The comparisons are performed independently for each month of composited data and for all eight months of data. The impact of any observed differences are illustrated within the context of a European forest/non-forest classification that utilizes NDVI and T_s data. All the analyses are performed independently for each forest stratum to reduce the impact of variations associated with the biophysical variables that were used to define the strata (climate, soil, topography, forest species, forest stand density). In all cases forest strata that contain less than nine forest pixels are not examined. This is to reduce the likelihood of mixed pixels which are assumed to be more likely in sparsely forested strata.

6.1. *Comparison of forest NDVI and* T_s *data extracted from monthly MaN and MaT composites*

Statistical tests are performed to characterize the form of any differences that may occur between NDVI values and also between T_s values extracted at the same forest locations from the MaN and MaT composites. The mean and the variance of the values are compared using a two independent sample T-test and a two independent sample difference of variance test respectively (DeGroot 1986). The tests are performed independently for each month of composited data and for each forest stratum.

One-tailed T-tests are used to establish if the mean forest NDVI is significantly greater when the NDVI data are extracted from the MaN or from the MaT

Table 2. The number of pairs of NDVI and T_s values extracted from the forest and non-forest pixels in each monthly MaN and MaT composite.

Monthly composite	Number of pairs extracted from the forest pixels	Number of pairs extracted from the non-forest pixels
March	23 909	33 032
April	26 518	36 917
May	23 398	34 498
June	27 731	38 437
July	27 539	36 967
August	29 007	39 112
September	26 024	35 597
October	24 654	32 553

composites. Difference of variance tests are used to establish if the forest NDVI variance is significantly greater when the NDVI data are extracted from the MaN or from the MaT composites. In this latter test an F-ratio is calculated by dividing the larger sample variance by the smaller sample variance to ensure that the F-ratio is always greater than or equal to one. The same tests are performed to compare the mean and the variance of forest T_s data extracted from the MaN and MaT composites.

6.2. *Average temporal separability of forest NDVI and* T_s *data extracted from different combinations of MaN and MaT composites*

Multi-temporal NDVI and T_s values have been shown for a given biome type to exhibit a seasonal trajectory related to changes in the temperature regime and the leaf cover (Lambin and Ehrlich 1996, Nemani and Running 1997). If the statistical distribution of forest NDVI and T_s values are sensitive to the compositing method it follows that the seasonal trajectory of the NDVI and T_s values may also be sensitive. This is investigated by examination of the average temporal separability between eight months of forest NDVI and T_s values extracted from different combinations of MaN and MaT composites.

Separability measures are used conventionally to describe the separation between the means and the distributions of two classes of data in a single index (Thomas *et al.* 1987). The Bhattacharyya distance (Fukunaga 1990) is used to measure separability as it does not require the data to be normalized, removing the requirement to make unverifiable assumptions concerning the relative importance of NDVI and T_s. The Bhattacharyya distance is known to be appropriate to separability problems where the distributions of the data are broad and is generally held to give similar results to other separability measures (Thomas *et al.* 1987). The Bhattacharyya distance is bounded between values of 0 (low separability) and 2 (high separability) and is monotonically related to classification accuracy when probability distribution class models (e.g., maximum likelihood) are used. In these cases a Bhattacharyya distance of 2·0 implies classification of pixel data into one of two classes with a 100 per cent classification accuracy.

Pairwise separabilities are computed between the eight months of forest NDVI and T_s data using the Bhattacharyya distance measure. For each month of NDVI and T_s data an average monthly separability is calculated as the mean of the seven pairwise separabilities between that month and the other seven months of data. Eight average monthly separabilities are calculated and their mean is taken to give a grand monthly average separability that is representative of the separability between all eight months of forest NDVI and T_s data. Higher grand monthly average separabilities will be found when the NDVI and T_s data have reduced variability within each month and increased separation between months. This procedure is repeated independently for each forest stratum and for the four possible ways that NDVI and T_s data can be extracted from MaN and MaT composites. These are: both NDVI and T_s extracted from MaN composites (combination 1), both NDVI and T_s values extracted from MaT composites (combination 2), NDVI values extracted from MaT composites and T_s values extracted from MaN composites (combination 3), and NDVI values extracted from MaN composites and T_s values extracted from MaT composites (combination 4). The combination that produces the highest grand monthly average separability can be inferred to be the most suitable for examination of the forest seasonal NDVI and T_s trajectory.

6.3. *Forest/non-forest classification*

The impact of using different combinations of MaN and MaT composites are illustrated within the context of a European forest/non-forest classification that uses NDVI and T_s data. Recently it has been suggested that the addition of T_s can discriminate regional land cover classes more effectively than NDVI alone (Running *et al.* 1994). This has been demonstrated using AVHRR data of the African continent (Ehrlich and Lambin 1996), of the conterminous U.S. (Nemani and Running 1997), and over Europe using the data described in this paper (Roy *et al.*, forthcoming). The biophysical justification for such a combination has been investigated in some detail by Lambin and Ehrlich (1996). Rather than produce many forest/non-forest classifications, the statistical separability between forest and non-forest NDVI and T_s data are calculated for each forest stratum using the Bhattacharyya distance. The four possible ways that NDVI and T_s data can be extracted from different combinations of MaN and MaT composites are examined. The combination of MaN and/or MaT composite data that produces the highest separability can be inferred to give the highest forest/non-forest classification accuracy.

7. Results

7.1. *Comparison of forest NDVI and* T_s *data extracted from monthly MaN and MaT composites*

Figure 1 illustrates the mean and the standard deviation of NDVI and T_s data extracted from the MaN and from the MaT monthly composites. The data are extracted from the same 500 forest pixels in a forest stratum lying in Les Landes region of S.W. France. This region contains dense stands of intensively managed *Pinus Pinaster*. Figure 1 (*a*) illustrates the NDVI summary statistics and figure 1 (*b*) illustrates the T_s summary statistics. Seasonal changes in the forest reflectance and thermal properties give an increase in NDVI and T_s towards the summer followed by decreasing values in the autumn months. The mean NDVI values are consistently higher and the standard deviation of the NDVI values are generally lower for the data extracted from the MaN rather than from the MaT composites (figure 1 (*a*)). Conversely, the mean T_s values are generally higher and the standard deviation of

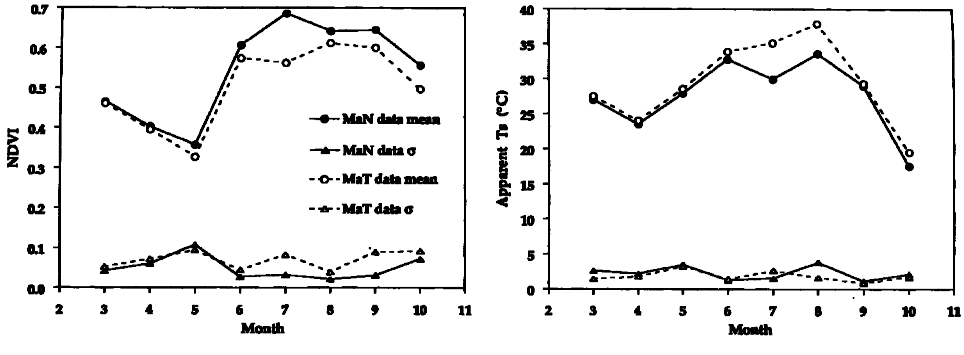

(*a*) (*b*)

Figure 1. Mean and standard deviation (σ) of NDVI and T_s forest pixel values extracted from monthly MaN and MaT composites. Figure 1 (*a*) NDVI summary statistics. Figure 1 (*b*) T_s summary statistics. The data are extracted from the same 500 forest pixels in a forest stratum lying in Les Landes region of south-west France.

the T_s values generally lower for the data extracted from the MaT rather than from the MaN composites (figure 1 (*b*)). These differences are most evident during the summer months. In July, the mean NDVI is approximately 0·1 higher when the NDVI data are extracted from the MaN rather than from the MaT composites. The mean T_s in July is approximately 5°C higher when the T_s data are extracted from the MaT rather than from the MaN composites. These data are analysed to test the significance of these observed differences. Figure 2 illustrates the results of two independent sample T-tests performed on a monthly basis between the NDVI data extracted from the MaN and from the MaT composites (figure 2 (*a*)) and between the T_s data extracted from the MaN and from the MaT composites (figure 2 (*b*)). Absolute values of the T-ratios are plotted with 90, 95 and 99 per cent confidence levels (for a one-tailed test) superimposed to aid interpretation. T-ratios on or above a confidence level indicate a significant difference at that confidence level. Figure 2 shows that the type of composite (MaN or MaT) significantly influences NDVI and T_s in all months except March, April and May. The temporal dependency of the differences observed in figure 1 are seen in the increasing T-ratio values in the summer months.

Tests of the differences between the NDVI data and between the T_s data extracted from the monthly MaN and MaT composites are performed for each forest stratum. The test results are inferred at the 95 per cent confidence level and are summarized in tables 3 and 4 for the difference of means and the difference of variance tests respectively. Only the percentage of forest strata that exhibit a significant difference are summarized because of the large number of tests performed. Tables 3 and 4 show that the NDVI data and the T_s data are significantly different when they are extracted from the MaN and the MaT composites for the *majority* of the forest strata. The differences are similar to those observed in figure 1, that is NDVI data extracted from the MaN composites have higher mean values and generally lower variances than NDVI data extracted from the MaT composites, whilst T_s data extracted from the MaT composites have higher mean values and generally lower variances than T_s data extracted from the MaN composites. The temporal dependency of the

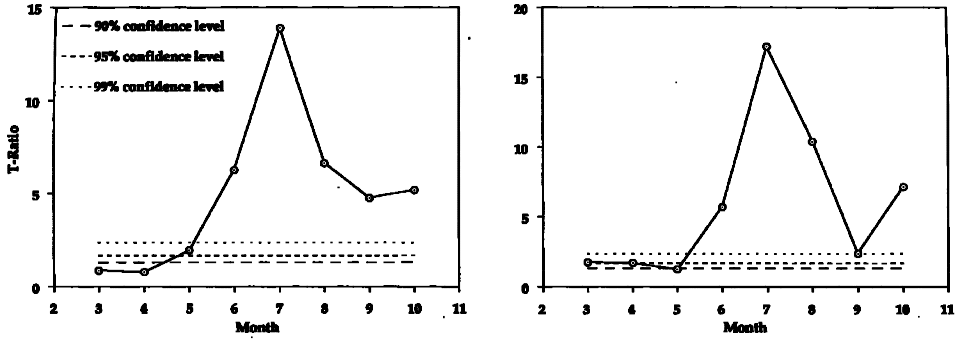

(*a*) (*b*)

Figure 2. Monthly two independent sample T-test results performed between forest NDVI data and between forest T_s data extracted from MaN and MaT composites. (*a*) T-ratios for NDVI data extracted from the MaN and from the MaT composites. (*b*) T-ratios for T_s data extracted from the MaN and from the MaT composites. The data are extracted from the same 500 forest pixels in a forest stratum lying in Les Landes region of south-west France.

Table 3. Percentage of European forest strata with significantly higher mean NDVI values and significantly higher mean T_s values when the NDVI data are extracted from maximum NDVI (MaN) and maximum T_s (MaT) monthly composites and when the T_s data are extracted from MaN and MaT monthly composites. Significance tests for each stratum are computed by comparison of between 9–500 forest pixel values using a two independent sample T-test. Test results are inferred at the 95·0 per cent confidence level for a one-tailed test. Percentages are quoted to the nearest decimal.

Monthly composite	% of forest strata with significantly higher mean NDVI values when NDVI extracted from:		% of forest strata with significantly higher mean T_s values when T_s extracted from:		Number of forest strata tested
	MaN	MaT	MaN	MaT	
March	71	0	0	73	72
April	87	0	0	80	77
May	64	0	0	54	77
June	88	0	0	88	76
July	89	0	0	88	76
August	96	0	0	97	77
September	88	0	0	83	76
October	73	0	0	74	77

Table 4. Percentage of European forest strata with significantly higher NDVI variances and significantly higher T_s variances when the NDVI data are extracted from maximum NDVI (MaN) and maximum T_s (MaT) monthly composites and when the T_s data are extracted from MaN and MaT monthly composites. Significance tests for each stratum are computed by comparison of between 9–500 forest pixel values using a difference of variance test for two independent samples. Test results are inferred at the 95·0 per cent confidence level. Percentages are quoted to the nearest decimal.

Monthly composite	% of forest strate with significantly higher NDVI variances extracted from:		% of forest strata with significantly higher T_s variances extracted from:		Number of forest strata tested
	MaN	MaT	MaN	MaT	
March	11	42	51	4	72
April	0	44	45	5	77
May	3	35	21	8	77
June	1	66	42	13	76
July	0	79	51	16	76
August	0	87	52	18	77
September	5	65	38	18	76
October	9	30	26	22	77

differences are evident. The percentage of strata with significantly higher mean NDVI values extracted from the MaN rather than from the MaT composites varies from 64 per cent (May) to 96 per cent (August) and the percentage of strata with significantly higher mean T_s values extracted from the MaT rather than from the MaN composites varies from 54 per cent (May) to 97 per cent (August). A similar, though less strong, temporal pattern is observed for the percentage of strata with significantly different NDVI and T_s variances.

7.2. *Average temporal separability of forest NDVI and* T_s *data extracted from different combinations of MaN and MaT composites*

Figure 3 illustrates T_s and NDVI data extracted from the same forest pixel locations from a forest stratum lying along the Mediterranean coastline in the Provence-Languedoc-Roussillon region of France. In each monthly composite a maximum of only 60 forest pixels could be extracted because of the sparseness of the forest cover which is characterized by thin-broken stands of mixed forest species. For reasons of clarity a sub-set of 24 pixels selected from the interiors of the largest forest regions are shown. Figure 3 illustrates the four possible ways that NDVI and T_s data can be extracted from different combinations of MaN and MaT composites. In each of these figures the monthly data form distinct clusters that exhibit a seasonal trajectory. The impact of extracting NDVI and T_s data from the different combinations of composited data are clearly evident in figure 3. Generally, NDVI data

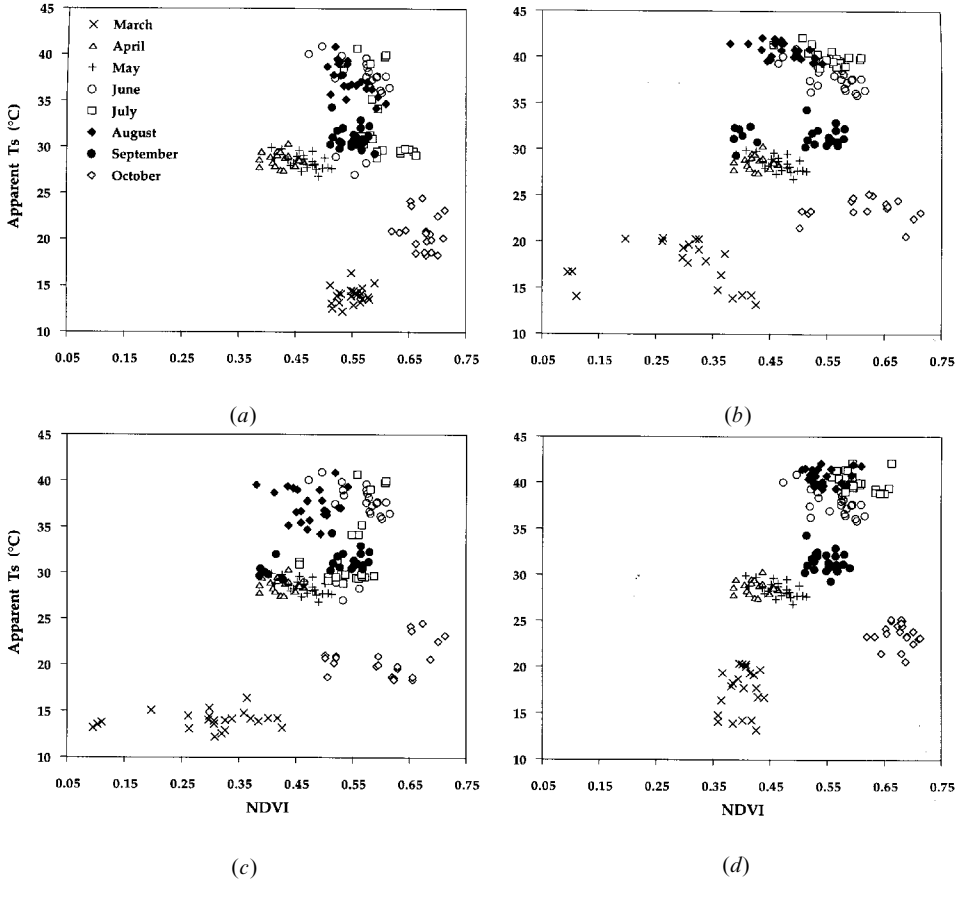

Figure 3. T_s and NDVI data extracted from the same 24 forest pixels from a forest stratum lying along the Mediterranean coastline in the Provence-Languedoc-Roussillon region of France. The four possible ways that NDVI and T_s data can be extracted from different combinations of MaN and MaT composites are illustrated. (*a*) NDVI and T_s values extracted from only the MaN composites. (*b*) NDVI and T_s values extracted from only the MaT composites. (*c*) NDVI values extracted from the MaT composites and T_s values extracted from the MaN composites. (*d*) NDVI values extracted from the MaN composites and T_s values extracted from the MaT composites.

extracted from the MaN composites appear to be more compactly clustered along the NDVI axis and higher valued than NDVI data extracted from the MaT composites. T_s data extracted from the MaT composites appear more compact in the T_s axis and higher valued than T_s data extracted from the MaN data.

The grand monthly average separabilities of the monthly NDVI and T_s data are calculated for each forest stratum and for each of the four combinations of composite data. Separabilities are only calculated for strata that contain nine or more of the same forest pixels in every monthly composite. In this way a total of 72 forest strata are examined. Summary statistics of the grand monthly average separabilities computed over the 72 strata and for the four combinations of composite data are shown in table 5. Examination of this table reveals a very clear pattern which supports the results described in §7.1. NDVI and T_s data extracted from the MaN and MaT

Table 5. Summary statistics of the grand monthly average separabilities computed over 72 forest strata. The grand monthly average separabilities are computed for each forest stratum from eight monthly clusters of NDVI and T_s data extracted from between 9–500 forest pixels. The NDVI and T_s data are extracted from different combinations of composite data: Combination (1) NDVI and T_s extracted from MaN composites, Combination (2) NDVI and T_s extracted from MaT composites, Combination (3) NDVI extracted from MaT and T_s extracted from MaN composites, Combination (4) NDVI extracted from MaN and T_s extracted from MaT composites. Separabilities are computed using the Bhattacharyya distance measure. Statistics are quoted to three decimal places.

	Minimum	Maximum	Mean	Standard deviation
Combination 1	0·881	1·827	1·283	0·205
Combination 2	0·794	1·767	1·297	0·211
Combination 3	0·689	1·705	1·123	0·235
Combination 4	0·899	1·869	1·372	0·198

Table 6. Mean and standard deviation (σ) of the forest/non-forest separabilities computed over all the forest strata for each month of composite data. Separabilities are computed for each forest stratum using NDVI and T_s extracted from between 9–500 forest and 9–500 non-forest pixels. These data are extracted from different combinations of composite data: Combination (1) NDVI and T_s extracted from MaN composites, Combination (2) NDVI and T_s extracted from MaT composites, Combination (3) NDVI extracted from MaT and T_s extracted from MaN composites, Combination (4) NDVI extracted from MaN and T_s extracted from MaT composites. Separabilities are computed using the Bhattacharyya distance measure. Statistics are quoted to three decimal places.

	Combination 1		Combination 2		Combination 3		Combination 4		Number of forest
Month	Mean	σ	Mean	σ	Mean	σ	Mean	σ	strata
March	0·341	0·232	0·421	0·243	0·322	0·221	0·435	0·251	72
April	0·407	0·270	0·442	0·298	0·382	0·257	0·475	0·317	77
May	0·439	0·274	0·435	0·281	0·413	0·260	0·458	0·297	77
June	0·506	0·331	0·512	0·338	0·459	0·322	0·573	0·357	76
July	0·600	0·392	0·505	0·335	0·462	0·326	0·652	0·394	76
August	0·621	0·374	0·517	0·339	0·466	0·333	0·685	0·377	77
September	0·575	0·383	0·525	0·331	0·496	0·320	0·638	0·397	76
October	0·405	0·306	0·364	0·293	0·368	0·285	0·417	0·313	77

composites respectively (combination 4) have the highest grand monthly average separabilities over all 72 strata (highest minimum, maximum, mean and lower standard deviation grand monthly average separabilities). Conversely, NDVI and T_s data extracted from the MaT and MaN composites respectively (combination 3) have the lowest grand monthly average separabilities (lowest minimum, maximum, mean and highest standard deviation grand monthly average separabilities). NDVI and T_s data extracted from only the MaN and from only the MaT composites (combinations 1 and 2 respectively) have separability results of intermediate and similar value.

7.3. *Forest/non-forest classification*

Separabilities are calculated between the forest and non-forest NDVI and T_s data selected from each forest stratum for each of the four possible combinations of MaN and MaT composites. Table 6 summarizes the mean and the standard deviation of the separabilities computed over all the strata for each month of composite data. The separabilities are quite low (less than 1·0) and imply that the monthly composite data would be classified into forest and non-forest classes with a low degree of accuracy. This is expected however as only a multi-temporal classification will properly capture seasonal variations. Further, the non-forest class encompasses all non-forest vegetation and soil cover types and will therefore be characterized by a very broad distribution of NDVI and T_s values. Also, the non-forest pixel values are not selected from areas of homogeneous land-cover where compositing errors caused by poor mosaic co-registration are likely to be less evident.

The separabilities summarised in table 6 illustrate the sensitivity of the potential forest/non-forest classification accuracy to the particular combination of MaN and/or MaT composite data and to the month of composite data that is used. For all the given combinations, the separabilities are highest in the summer months. NDVI and T_s data extracted from the MaN and MaT composites respectively (combination 4) have the highest mean and standard deviation separabilities for every month of

Table 7. Percentage of forest strata that have lower forest/non-forest separabilities when NDVI and T_s data are extracted from different combinations of composite data compared to those computed using data extracted from Combination 4. The different combinations of composite data: Combination (1) NDVI and T_s extracted from MaN composites, Combination (2) NDVI and T_s extracted from MaT composites, Combination (3) NDVI extracted from MaT and T_s extracted from MaN composites, Combination (4) NDVI extracted from MaN and T_s extracted from MaT composites. Separabilities are computed using the Bhattacharyya distance measure. Separabilities are computed for each forest stratum using NDVI and T_s extracted from between 9–500 forest and 9–500 non-forest pixels. Percentages are quoted to the nearest decimal.

Month	Combination 1	Combination 2	Combination 3	Number of forest strata
March	78	60	76	72
April	69	73	74	77
May	65	67	77	77
June	71	80	79	76
July	71	83	87	76
August	81	83	97	77
September	72	79	83	76
October	56	71	71	77

composite data. Conversely, NDVI and T_s data extracted from the MaT and MaN composites respectively (combination 3) have the lowest mean and standard deviation separabilities for almost every month. NDVI and T_s data extracted from only the MaN and from only the MaT composites (combinations 1 and 2 respectively) have intermediate and similar separability statistics. The consistently high mean separabilities found with combination 4 are offset by their high variability. However, the majority of the forest strata exhibit higher forest/non-forest separabilities for combination 4 than for any of the other combinations. This is shown in table 7 which summarizes the percentage of forest strata that have lower forest/non-forest separabilities for the first three combinations of composite data compared to combination 4. These results imply that a European forest/non-forest classification should use NDVI data extracted from MaN composites and T_s data extracted from MaT composites.

8. Conclusions

The impact of the maximum Normalized Difference Vegetation Index (NDVI) and the maximum surface temperature (T_s) compositing procedures (MaN and MaT respectively) upon retrieved NDVI and T_s values extracted from cloud-screened European AVHRR LAC data have been investigated. The statistical distributions of forest NDVI and T_s values have been analysed with respect to contiguous strata that characterize different ecological/climatic regions and forest types within Europe. The MaN and MaT compositing procedures have been shown to influence significantly the distributions of the NDVI and T_s values for the majority of the strata. NDVI values are observed to be higher and generally less variable when they are extracted from MaN rather than from MaT composites and T_s values are observed to be higher and generally less variable when they are extracted from MaT rather than from MaN composites. Further work is required to establish if similar results are found for non-forest cover types and in ecological regions with different climatic regimes outside of Europe. These findings have been illustrated within the context of a European forest/non-forest classification that uses NDVI and T_s data. Examination of forest/non-forest separabilities indicate that the potential classification accuracies are sensitive to the combination of MaN and/or MaT composite data that is used. In order to maximise the separability between forest and non-forest classes, and therefore to ensure higher potential forest/non-forest classification accuracies, the results indicate that NDVI data should be extracted from MaN composites and that T_s data should be extracted from MaT composites.

The findings of this investigation indicate that inappropriate selection of a compositing procedure may have a significant impact upon the subsequent application of NDVI and/or T_s data. They imply that caution must be applied in the quantitative analysis of T_s data extracted from MaN composites and in the quantitative analysis of NDVI data extracted from MaT composites. However, the recommendations are formulated only by examination of NDVI and T_s values extracted from cloud-screened MaN and MaT composites. The observed variations in the NDVI and T_s values may also have been influenced by other factors that were not investigated. These include inadequacies in the cloud screening algorithm, different biases in the atmospheric correction of the reflected and emitted wavelengths where the NDVI and T_s are measured respectively, and different bidirectional effects at the reflected and emitted wavelengths. The results of this investigation should be confirmed by more theoretically based research in these respects.

The findings of this investigation may be particularly relevant to those applications that utilise both NDVI and T_s data. For example, NDVI and T_s have been used for studies of soil moisture, evapotranspiration and surface energy fluxes (Goward and Hope 1989, Carlson *et al.* 1990, Nemani *et al.* 1993), for land cover mapping (Ehrlich and Lambin 1996, Nemani and Running 1997), and for change detection (Lambin and Strahler 1994, Lambin and Ehrlich 1996). However, the extraction of NDVI and T_s data from independently composited images has certain disadvantages. NDVI and T_s values extracted at the same pixel location from MaN and MaT composites may originate from *different* images sensed at different times within the compositing period. This may introduce problems of data interpretation particularly if the time scales of variation of NDVI and T_s are significantly different. Variations in the slope of T_s and NDVI have been interpreted biophysically in terms of regional surface resistance to evapotranspiration and as a method for capturing information related to the fractional green vegetation cover (Nemani *et al.* 1993). Variations in NDVI are driven largely by seasonal changes in the rates of vegetation activity while variations in T_s in semi-arid or dry subhumid ecosystems, where the fractional green vegetation cover is low, are driven mainly by rainfall events (Lambin and Strahler 1994). It may therefore be more meaningful to use different compositing periods to produce the MaN and MaT composites. Further research is required to investigate the interrelationship between the compositing period and the rate of change of the defined measure used to composite the data.

Acknowledgments

The comments of Eric Lambin on this manuscript are greatly appreciated. The author would like to thank the JRC MARS project for provision of the European AVHRR mosaics used in the study.

References

Breaker, L., 1990, Estimating and removing sensor-induced correlation from advanced very high resolution radiometer satellite data. *Journal of Geophysical Research*, **95,** 9701–9711.

Carlson, T. N., Dodd, J. K., Benjamin, S. G., and Cooper, J. N., 1981, Remote estimation of surface energy balance, moisture availability and thermal inertia. *Journal of Applied Meteorology*, **20,** 67–87.

Carlson, T. N., Perry, E. M., and Schmugge, T. J., 1990, Remote estimation of soil moisture availability and fractional vegetation cover for agricultural fields. *Agricultural and Forest Meteorology*, **52,** 45–69.

Cihlar, J., 1987, Environmental factors influencing day time and night time satellite thermal infrared images. *Canadian Journal of Remote Sensing*, **13,** 31–38.

Cihlar, J., 1994, Detection and removal of cloud contamination from AVHRR images. *I.E.E.E. Transactions on Geoscience and Remote Sensing*, **32,** 583–589.

Cihlar, J., Manak, D., and D'Iorio, M., 1994 a, Evaluation of compositing algorithms for AVHRR data over land. *I.E.E.E. Transactions on Geoscience and Remote Sensing*, **32,** 427–437.

Cihlar, J., Manak, D., and Voisin, N., 1994 b, AVHRR bidirectional reflectance effects and compositing. *Remote Sensing Environment*, **48,** 77–88.

Choudhury, B. J., 1989, Estimating evaporation and carbon assimilation using infrared temperature data: vistas in modelling. In *Theory and Applications of Optical Remote Sensing*, edited by G. Asar (New York: John Wiley and Sons), pp. 628–690.

Curran, P. J., 1983, Multispectral remote sensing for estimation of green leaf area index. *Philosophical Transactions of the Royal Society, Series A*, **309,** 257–270.

Davis, P., Stowe, L., and McClain, E., 1993, Development of a cloud layer detection algorithm for the clouds from AVHRR (CLAVR) phase II code. *Proceedings SPIE*

Conference on Passive Infrared Remote Sensing of Cloud and the Atmosphere, Volume 1934 (Bellingham, WA: SPIE), pp. 36–48.

DeFries, R. S., and Townshend, J. R. G., 1994, NDVI-derived land cover classification at a global scale. *International Journal of Remote Sensing*, **15,** 3567–3586.

DeGroot, M. H., 1986, *Probability and Statistics* (Reading, MA: Addison-Wesley Publishing Company), pp. 437–512.

D'Iorio, M. A., Cihlar, J., and Morasse, C. R., 1991, Effect of the calibration of AVHRR data on the normalised difference index and compositing. *Canadian Journal of Remote Sensing*, **17,** 251–262.

Ehrlich, D., and Lambin, E. F., 1996, Broad scale land-cover classification and interannual climatic change. *International Journal of Remote Sensing*, **17,** 845–862.

Epiphanio, J. C. N., and Huete, A. R., 1995, Dependence of NDVI and SAVI on sun/sensor geometry and its effect on fAPAR relationships in Alfalfa. *Remote Sensing of Environment*, **51,** 351–360.

ESRI, 1993, *The Digital Chart of The World*, Environmental Systems Research Inc., 380 New York Street, Redlands, CA 92373, U.S.A.

European Commission, 1995, Regionalization and Stratification of European Forest Ecosystems, Internal Special Publication of the Joint Research Centre of the European Commission. S.P.I.95.44, European Commission Joint Research Centre, Institute for Remote Sensing Applications, Environmental Mapping and Modelling Unit, Italy.

Fukunaga, K., 1990, *Introduction to Statistical Pattern Recognition*, Second Edition (London: Academic Press Inc).

Gates, D. M., 1980, *Biophysical Ecology* (New-York: Springer-Verlag).

Goward, S. N., Cruickshanks, G. D., and Hope, A. S., 1985, Observed relation between thermal emission and reflected spectral radiance of a complex vegetated landscape. *Remote Sensing of Environment*, **18,** 137–146.

Goward, S. N., and Dye, D. G., 1987, Evaluating North American net primary productivity with satellite observations. *Advances in Space Research*, **7,** 165–174.

Goward, S. N., and Hope, A. S., 1989, Evapotranspiration from combined reflected solar and emitted terrestrial radiation: Preliminary FIFE results from AVHRR data. *Advances in Space Research*, **9,** 239–249.

Goward, S. N., Markham, B., Dye, D. G., Dulaney, W., and Yang, J., 1991, Normalized difference vegetation index measurements from the advanced very high resolution radiometer. *Remote Sensing of the Environment*, **35,** 257–277.

Gutman, G., 1987, The derivation of vegetation indices from AVHRR data. *International Journal of Remote Sensing*, **8,** 1235–1243.

Hausler, T., Saradeth, S., and Amitai, Y., 1993, NOAA-AVHRR forest map of Europe. *Proceedings of the International Symposium Operationalization of Remote Sensing, 19–23 April, ITC Enschede, The Netherlands* (Enshede: International Institute for Aerospace Survey and Earth Sciences), pp. 37–48.

Holben, B. N., 1986, Characteristics of maximum-value composite images from temporal AVHRR data. *International Journal of Remote Sensing*, **7,** 1417–1434.

Holben, B. N., and Justice, C. O., 1981, An examination of spectral band ratioing to reduce the topographic effect on remotely sensed data. *International Journal of Remote Sensing*, **2,** 115–133.

Justice, C. O., Townshend, J. R., Holben, B. N., and Tucker, C. J., 1985, Analysis of the phenology of global vegetation using meteorological satellite data. *International Journal of Remote Sensing*, **6,** 1271–1381.

Kaufman, Y., 1989, The atmospheric effects on remote sensing and its correction, In *Theory and Applications of Optical Remote Sensing*, edited by G. Asar (New York: John Wiley and Sons), pp. 336–428.

Labed, J., and Stoll, M. P., 1991, Angular variation of land surface spectral emissivity in the thermal infrared: laboratory investigations on bare soils. *International Journal of Remote Sensing*, **12,** 2299–2310.

Lambin, E. F., and Ehrlich, D., 1996, The surface temperature-vegetation index space for land cover and land-cover change analysis. *International Journal of Remote Sensing*, **17,** 463–478.

Lambin, E. F., and Strahler, A. H., 1994, Indicators of land cover change for change vector analysis in multitemporal space at coarse spatial scales. *International Journal of Remote Sensing*, **10,** 2099–2119.

Liu, H. Q., and Huete, A. R., 1995, A feedback based modification of the NDVI to minimize canopy background and atmospheric noise. *I.E.E.E. Transactions on Geoscience and Remote Sensing*, **33,** 457–465.

Los, S. O., Justice, C. O., and Tucker, C. J., 1994, The global 1° by 1° NDVI data set for climate studies derived from the GIMMS continental NDVI data. *International Journal of Remote Sensing*, **15,** 3493–3518.

Loveland, T., Merchant, J., Ohlen, D., and Brown, J., 1991, Development of a land-cover characteristics database for the conterminous U.S. *Photogrammetric Engineering and Remote Sensing*, **57,** 1453–1463.

Meyer, D., Verstraete, M., and Pinty, B., 1995, The effect of surface anisotropy and viewing geometry on the estimation of NDVI from AVHRR. *Remote Sensing Reviews*, **12,** 3–27.

Meyer-Roux, J., and Vossen, P., 1993, The first phase of the MARS project, 1988–1993: overview, methods and results. *Proceedings of Conference on The MARS Project: Overview and Perspectives, Institute for Remote Sensing Applications, Villa Carlotta, Belgirate, Lake Maggiore, Italy, 17–18 November, 1993* (Luxembourg: European Commission EUR 15599 EN), pp. 33–81.

Moody, A., and Strahler, A., 1994, Characteristics of composited AVHRR data and problems in their classification. *International Journal of Remote Sensing*, **15,** 3473–3491.

Muirhead, K., and Malkawi, O., 1989, Automatic classification of AVHRR images. *Proceedings of the Fourth AVHRR Data Users Meeting, Rottenburg, Germany, 5–8 September 1989* (Darmstadt-Eberstadt: EUMETSAT, am Elfengrund 45, D-6100), pp. 31–34.

Nemani, R. R., Pierce, L., Running, S. W., and Goward, S., 1993, Developing satellite derived estimates of surface moisture status. *Journal of Applied Meteorology*, **32,** 548–557.

Nemani, R., and Running, S., 1997, Land cover characterisation using multitemporal red, near-ir and thermal-ir data from NOAA/AVHRR. *Ecological Applications*, **7,** 79–90.

Norman, J. M., Divakarla, M., and Goel, N. S., 1995, Algorithms for extracting information from remote thermal-IR observations of the earth's surface. *Remote Sensing of Environment*, **51,** 157–168.

Pech, R., and Davis, A., 1987, Reflectance modelling of semiarid woodlands. *Remote Sensing of the Environment*, **23,** 365–377.

Pinty, B., and Verstraete, M., 1992, On the design and validation of bidirectional reflectance and albedo models. *Remote Sensing of Environment*, **41,** 155–167.

Price, J., 1984, Land surface temperature measurements from the split window channels of the NOAA 7 advanced very high resolution radiometer. *Journal of Geophysical Research*, **89,** 7231–7237.

Prince, S., and Tucker, C., 1986, Satellite remote sensing of rangelands in Botswana II. NOAA AVHRR and herbaceous vegetation. *International Journal of Remote Sensing*, **7,** 1555–1570.

Rao, C. R., and Chen, J., 1994, Post-launch calibration of the visible and near-infrared channels of the advanced very high resolution radiometer on NOAA-7, -9 and -11 spacecraft, NOAA Technical Report NESDIS 78, Washington, D.C.

Roy, D., Kennedy, P., and Folving, S., 1997, Combination of the normalised difference vegetation index and surface temperature for regional scale European forest cover mapping using AVHRR data. *International Journal of Remote Sensing*, **18,** 1189–1195.

Running, S. W., and Nemani, R. R., 1988, Relating seasonal patterns of the AVHRR vegetation index to simulated photosynthesis and transpiration of forests in different climates. *Remote Sensing of Environment*, **24,** 347–367.

Running, S. W., Justice, C. O., Salomonson, V., Hall, D., Barker, J., Kaufman, Y. J., Strahler, A. H., Huete, A. R., Muller, J.-P., Vanderbilt, V., Wan, Z. M., Teillet, P., and Carneggie, D., 1994, Terrestrial remote sensing science and algorithms planned for EOS/MODIS. *International Journal of Remote Sensing*, **15,** 3587–3620.

SAUNDERS, R. W., and KRIEBEL, K. T., 1988, An improved method for detecting clear sky and cloudy radiances from AVHRR data. *International Journal of Remote Sensing*, **9,** 123–150.

SELLERS, P., 1985, Canopy reflectance, photosynthesis and transpiration. *International Journal of Remote Sensing*, **6,** 1335–1372.

SERRA, J., 1986, Introduction to mathematical morphology. *Computer Vision Graphics and Image Processing*, **35,** 283–305.

TACONET, O., CARLSON, T. N., BERVARD, R., and VIDAL-MADJAR, D., 1986, Evaluation of a surface/vegetation parameterization using satellite measurements of surface temperature. *Journal of Climate and Applied Meteorology*, **25,** 1752–1767.

TANRÉ, D., DEROO, C., DUHAUT, P., HERMAN, M., MORCRETTE, J., PERBOS, J., and DESCHAMPS, P., 1990, Description of a computer code to simulate the satellite signal in the solar spectrum: the 5S code. *International Journal of Remote Sensing*, **11,** 659–668.

THOMAS, I. L., BENNING, V. M., and CHING, N. P., 1987, *Classification of Remotely Sensed Images* (Bristol: Hilger) pp. 82–101.

TOWNSHEND, J. R., JUSTICE, C. O., and KALB, V., 1987, Characterisation and classification of South American land cover types using satellite data. *International Journal of Remote Sensing*, **8,** 1189–1207.

TOWNSHEND, J. R., JUSTICE, C. O., GURNEY, C., and MCMANUS, J., 1992, The impact of misregistration on change detection. *I.E.E.E. Transactions on Geoscience and Remote Sensing*, **30,** 1054–1060.

TUCKER, C. J., HOLBEN, B. N., ELGIN, J. H., and MCMURTY, J. E., 1981, Remote sensing of total dry matter accumulation in winter wheat. *Remote Sensing of Environment*, **11,** 171–189.

TUCKER, C., GATLIN, J., and SCHNEIDER, S., 1984, Monitoring vegetation in the Nile delta with NOAA-6 and NOAA-7 AVHRR imagery. *Photogrammetric Engineering and Remote Sensing*, **50,** 53–61.

TUCKER, C. J., VANPRAET, C. L., SHARMAN, M. J., and VAN ITTERSUM, G., 1985, Satellite remote sensing of total herbaceous biomass production in Senegalese Sahel: 1980–1984. *Remote Sensing of Environment*, **17,** 233–249.

VERMOTE, E. F., TANRÉ, D., DEUZE, J. L., HERMAN, M., and MORCRETTE, J. J., 1997, Second simulation of the satellite signal in the solar spectrum: An overview. *I.E.E.E. Transactions on Geoscience and Remote Sensing*, in press.

VOGT, J. V., 1995, Land surface temperature retrieval from NOAA AVHRR data, In *Advances in the Use of NOAA AVHRR Data for Land Applications*, edited by G. D'Souza, A. Belward and J. P. Malingreau (Dordrecht, Boston, London: Kluwer Academic Publishers), pp. 125–152.

VOWLES, G., 1991, Space: Software to preprocess AVHRR data. *Proceedings of Conference on The Application of Remote Sensing to Agricultural Statistics, Institute for Remote Sensing Applications, Villa Carlotta, Belgirate, Lake Maggiore, Italy, 26–27 November, 1991* (Luxembourg: European Commission EUR 14262 EN), pp. 209–217.

WAN, Z., and DOZIER, J., 1989, Land-surface temperature measurement from space: physical principals and inverse modelling. *I.E.E.E. Transactions on Geoscience and Remote Sensing*, **27,** 268–277.